






Article

Integrated Biochar–Compost Amendment for *Zea mays* L. Phytoremediation in Soils Contaminated with Mining Tailings of Quiulacocha, Peru

Paul Virú-Vasquez ^{1,*} , Alex Pilco-Nuñez ² , Freddy Tineo-Cordova ², César Toribio Madueño-Sulca ², Teodosio Celso Quispe-Ojeda ³, Antonio Arroyo-Paz ⁴ , Ruby Alvarez-Arteaga ⁵, Yessenia Velasquez-Zuñiga ⁶, Luis Lizardo Oscanoa-Gamarra ⁷, Juan Saldivar-Villarroel ⁸ , Mary Flor Césare-Coral ⁹  and Ever Nuñez-Bustamante ¹⁰

¹ Faculty of Environmental Engineering and Natural Resources, Universidad Nacional del Callao, Callao 07011, Peru

² Faculty of Chemical and Textile Engineering, Universidad Nacional de Ingeniería, Lima 15024, Peru; apilco@uni.edu.pe (A.P.-N.); ftineo@uni.edu.pe (F.T.-C.); cesar.madueno.s@uni.edu.pe (C.T.M.-S.)

³ Faculty of Environmental Engineering, Universidad Nacional de Ingeniería, Lima 15024, Peru; tquispeo@uni.edu.pe

⁴ Facultad de Ingeniería, Universidad Tecnológica del Perú, Lima 15024, Peru; c25921@utp.edu.pe

⁵ Facultad de Ingeniería Geológica y Metalúrgica, Universidad Nacional del Altiplano, Puno 21001, Peru; ralvarez@unap.edu.pe

⁶ Facultad de Ingeniería Química, Universidad Nacional del Altiplano, Puno 21001, Peru; yessenia.velasquez@unap.edu.pe

⁷ Programa de Investigación Formativa, Universidad César Vallejo, Lima 15024, Peru; loscanoaga@ucvvirtual.edu.pe

⁸ Facultad de Agronomía, Universidad Nacional de Cañete, Lima 15024, Peru; jsaldivar@undc.edu.pe

⁹ Faculty of Sciences, Universidad Nacional Agraria La Molina, Lima 15024, Peru; mcesare@lamolina.edu.pe

¹⁰ Faculty of Agricultural Sciences, Universidad Nacional Autónoma de Chota, Chota 06121, Peru; enunezb@unach.edu.pe

* Correspondence: phviruv@unac.edu.pe



Academic Editors: Valeria Spagnuolo and Genxing Pan

Received: 5 March 2025

Revised: 24 April 2025

Accepted: 8 May 2025

Published: 12 May 2025

Citation: Virú-Vasquez, P.; Pilco-Nuñez, A.; Tineo-Cordova, F.; Madueño-Sulca, C.T.; Quispe-Ojeda, T.C.; Arroyo-Paz, A.; Alvarez-Arteaga, R.; Velasquez-Zuñiga, Y.; Oscanoa-Gamarra, L.L.; Saldivar-Villarroel, J.; et al. Integrated Biochar–Compost Amendment for *Zea mays* L. Phytoremediation in Soils Contaminated with Mining Tailings of Quiulacocha, Peru. *Plants* **2025**, *14*, 1448. <https://doi.org/10.3390/plants14101448>

Copyright: © 2025 by the authors. Licensee MDPI, Basel, Switzerland. This article is an open access article distributed under the terms and conditions of the Creative Commons Attribution (CC BY) license (<https://creativecommons.org/licenses/by/4.0/>).

Abstract: This study evaluated the phytoremediation of mine tailing-contaminated soils in Quiulacocha, Peru, using the combined application of biochar and compost, with *Zea mays* L. (maize) serving as the phytoremediator due to its high biomass production and stress tolerance. A factorial experimental design was implemented, varying two main factors: the mining tailings dose (30% and 60% *w/w*) and the biochar pyrolysis temperature (300 °C and 500 °C). The mine tailings were characterized by high concentrations of heavy metals and unfavourable physico-chemical properties (pH, low organic matter), whereas the biochar, produced from pine forest residues, and the compost, derived from urban organic waste, exhibited attributes that enhance soil quality. During the pot experiment, response variables including the Bioconcentration Factor (BCF) and Translocation Factor (TF) for various metals were evaluated to assess the capacity for contaminant immobilization and their distribution between plant roots and aerial tissues. The results demonstrated that the incorporation of biochar and compost significantly improved soil quality by increasing pH, cation exchange capacity, and nutrient retention, while simultaneously reducing the bioavailability of heavy metals and limiting their translocation to the aerial parts of maize. Factorial analysis further indicated that both the tailings dose and biochar pyrolysis temperature significantly influenced the efficacy of the phytoremediation process. In conclusion, the combined application of biochar and compost presents an effective and sustainable strategy for rehabilitating mine tailing-contaminated soils by stabilizing heavy metals and promoting the safe growth of *Zea mays* L.

Keywords: biochar; compost; mine tailings; phytoremediation; *Zea mays* L.

1. Introduction

Large-scale mining generates massive volumes of mine tailings (fine waste from mineral processing), estimated at over 14 billion tons annually worldwide [1], generating pollution, specifically affecting the soil in many countries worldwide, including China [2], Australia [3], Spain [4], South Africa [5], Mexico [6], and Peru [7,8]. In Latin America, numerous Mining Environmental Liabilities (MELs) have been documented, notably in countries such as Ecuador [9], Peru [10], Colombia [11], and Chile [12]. MELs often result from abandoned or inadequately managed mining operations, posing ongoing environmental and health risks to surrounding communities. Addressing these liabilities is crucial for sustainable development and the protection of ecosystems in the region. These wastes contain high concentrations of toxic heavy metals, such as cadmium (Cd), lead (Pb), zinc (Zn), copper (Cu), chromium (Cr), nickel (Ni), and arsenic (As), among others [13].

Improper disposal of mine tailings enables metal-rich particles to migrate kilometres from the source via erosion and leaching, polluting soils and water bodies [14]. Heavy-metal enrichment disrupts soil biota, suppressing beneficial microbes, harming fauna, and destabilizing ecosystem functions [15], while the persistence and bioaccumulative nature of many metals permits their entry into food webs, creating chronic human health risks [16]. Remediation is particularly challenging because tailing-impacted soils are acidic, compact, nutrient-poor, and low in organic matter, conditions hostile to plant establishment [17]. Organic amendments have therefore been advocated to upgrade soil quality and attenuate in situ metal toxicity [18]. Compost supplies stabilized organic matter and nutrients that boost microbial activity and improve soil structure, aeration, and water retention, thus fostering vegetation recovery [19,20]. Biochar, a porous, carbon-rich pyrolysate, adds a high surface area, functional groups, and alkalinity, allowing it to adsorb and immobilize metals while conditioning the soil's physical, chemical, and biological attributes [21–23]. Recent work shows that combining compost and biochar magnifies these individual benefits [24–26]: corn-straw biochar in sludge compost cut metals and antibiotic-resistance genes by up to 97.9% [27]; co-composting plant residues with biochar accelerated humification and generated a high-quality peat substitute [28]; biochar-compost blends in pesticide-laden soils under freeze–thaw cycles enhanced degradation and soil multifunctionality [29]; and earthworm-assisted sludge composting with biochar shifted cadmium into less mobile fractions and lowered associated resistance genes [30].

Phytoremediation harnesses plants to rehabilitate contaminated soils in situ, offering a low-cost and environmentally benign alternative to physicochemical methods [31]. For heavy-metal pollution, it operates chiefly through two distinct, yet complementary, mechanisms. Phytoextraction involves (i) the root uptake of soluble or weakly sorbed metal ions, (ii) xylem-mediated translocation, and (iii) sequestration in harvestable above-ground biomass; repeated cropping and biomass removal gradually deplete the contaminant pool [32]. Phytostabilization, by contrast, immobilizes metals in the root zone: root exudates and rhizosphere microbes raise pH, supply organic ligands, or promote the formation of carbonate, phosphate, and sulphide precipitates, while biochar- or compost-induced surface functional groups adsorb complex cations; the resulting reduction in metal solubility and dust generation curtails their ecological and human exposure [33]. Successful application demands species that grow rapidly, generate ample biomass, and tolerate metal stress [34]. The *Zea mays* L. satisfies the key attributes for metal phytoremediation high biomass, agronomic familiarity, broad climatic adaptability, and proven metal tolerance and has already been deployed both for phytoextraction [35] and phytostabilization [36].

Recent evidence reinforces its suitability: Atta et al. showed maize cultivars removing up to 38% Cr and 24% Pb while sustaining growth under 300 ppm stress [37]; Ahmad [38] demonstrated that P-loaded biochar co-applied with maize cut the exchangeable Cd, Pb, Cu, and Zn fractions and boosted shoot biomass two to three fold; Rosas-Castor [39] reviewed the capacity of the plants to take up and translocate arsenic, highlighting its importance where As-laden irrigation water is common. Field and pot studies in tropical soils echo these findings: biochar-amended maize improved height and dry matter while lowering soil Cu/Zn availability after 22 years of industrial contamination, and lysimeter trials recorded meaningful Cd and Zn extraction without growth penalties. Maize has also been classified as a Cr (VI) hyper accumulator under chelate-assisted conditions, with shoot concentrations rising tenfold over controls, and comprehensive reviews position it among the most promising high biomass candidates for large-scale, low-cost phytoremediation programmers. Collectively, these studies confirm that maize not only tolerates but actively removes a broad spectrum of priority metals while retaining the practical advantages of seed availability, local acceptance, and established agronomy that make it logistically attractive for remediation projects [40,41].

Growing evidence indicates that amending contaminated soils with biochar [1], compost [42] or, most effectively, their combined application can enhance phytoremediation by improving soil physical structure, increasing cation exchange capacity, and supplying essential nutrients [43]. Biochar–compost blends have successfully reduced the bioavailability of Cd and Zn [44,45] and stabilized Pb and As [46], while *Zea mays* L. has been widely investigated as a phytoextractor of Cu [47], Zn [47,48], Pb [49–51], and Cr [52]. In tropical field trials, integrated biochar–compost strategies improved soil water retention, boosted cation exchange capacity, and raised maize grain yields by 10–29% [24–27]. Complementary pot experiments confirmed that the co-application of the two amendments alleviates Cr phytotoxicity in maize by enhancing morphophysiological and biochemical traits [53], lowers the bioavailability and plant uptake of Cr, Ni, Pb, and Zn while stimulating biomass production, and, when combined with maize straw, modifies root exudation patterns in ways that further enrich soil fertility and yield [54]. Additional studies have shown that agro-industrial biochar–compost mixtures increase P availability and organic matter content in acidic soils, thereby optimizing maize performance [55], and that integrating these organic amendments with manures mitigates Ni toxicity, sustains photosynthesis, and promotes overall plant efficiency [56]. Nonetheless, maize-based phytoremediation is not without its caveats: several reports document appreciable Cd, Pb, and Zn transfer to kernels and fodder, raising food safety concerns; consequently, harvested biomass should be channelled to non-edible uses (e.g., bioenergy or fibre) and grain metal concentrations must be routinely monitored to ensure regulatory compliance [57].

Peru's Quiulacocha mining tailings (QMT) deposit, created in 1930 by the Copper Corporation and now classified as an MEL unchecked disposal of pyrite-rich tailings (~50% pyrite) around an acid lagoon, has long harmed local ecosystems and nearby communities [58–60]. Recent climate data underline the urgency of intervention: extraordinary storms in 2021 dropped >10 mm day⁻¹ of rain, shrinking the tailings' freeboard to just 55 cm [61]; in 2022, 13.2 mm day⁻¹ rainfall reduced it further to 61 cm; and intense 2023 downpours in districts such as Paucartambo confirm a continuing trend [62]. These events heighten the risk that rivers bordering the site—the Ragra and San Juan—along with adjacent soils will become conduits for heavy-metal dispersion, threatening environmental and human health through contaminated water, food chains, and direct soil contact. The magnitude of contamination caused by the Quiulacocha mine tailings in Junín, Peru, necessitates comprehensive, effective, and sustainable environmental remediation strategies. In this

context, the combination of organic amendments with phytoremediation using *Zea mays* L. emerges as a promising solution for rehabilitating soils with high levels of heavy metals.

Therefore, this study focuses on evaluating the effectiveness of using biochar, compost, and *Zea mays* L. in the remediation of soil contaminated with mine tailings from Quiulacocha, providing valuable insights for the treatment of mining environmental liabilities and the mitigation of their ecosystem impacts.

2. Results and Discussion

2.1. Mine Tailing Physicochemical Characterization

The Quiulacocha mine tailings in Peru cover approximately 114 hectares and consist of roughly 79 Mt of tailings, containing about 50% pyrite by weight [63]. Mineralogical surveys report that the solid phase is dominated by sulphide minerals, principally pyrite (FeS_2 , 50–60 wt%) with accessory pyrrhotite and marcasite which oxidize to generate acid mine drainage [64]. Consistent with this assemblage, bulk chemistry shows very high total concentrations of Zn (9091 mg kg^{-1}), Pb (3984 mg kg^{-1}), and As (1015 mg kg^{-1}) (Table 1), while the matrix remains poorly buffered (CaCO_3 0.35%) and low in organic matter (3.02%), leading to an acidic pH of 5.63 and elevated electrical conductivity (7.14 mS cm^{-1}). These mineralogical and geochemical features confirm the high acid-generating potential and metal mobility of the deposit, underpinning the rationale for testing alkaline, functional-group-rich biochar–compost amendments to raise pH and immobilize metals in situ. For the physicochemical characterization of mining tailings that is shown, the content of organic matter (OM) is important since it can enhance metal adsorption in a tailing’s plant–soil environment [65]. The pH was acidic, and this could be due to the tailings containing more acidic minerals instead of minerals with a neutralization capacity (carbonates and hydroxides) [66]. Furthermore, if the mine tailings exhibit acidity, this will lead to a reduction in the ability of the soil to exchange metal cations and an elevation in metal solubility [67]. Also, the content of P (ppm), K (ppm), CaCO_3 (%), and EC is shown.

Table 1. Physicochemical characterization of the Quiulacocha mining tailings.

| Heavy Metals in Mining Tailings | | | | | | |
|--|-------------|---------------------|---------------|-------------|-----------------|--------------------|
| As (mg/kg) | Cd (mg/kg) | Cr (mg/kg) | Cu (mg/kg) | Ni (mg/kg) | Pb (mg/kg) | Zn (mg/kg) |
| 1015.33 ± 5.03 | 17 ± 1.00 | 40.67 ± 0.58 | 288.30 ± 1.57 | 9.60 ± 0.53 | 3983.67 ± 29.50 | 9091.00 ± 79.96 |
| Physicochemical Characteristics of Mining Tailings | | | | | | |
| pH | EC | CaCO_3 (%) | OM (%) | P (ppm) | K (ppm) | C.E.C. (meq/100 g) |
| 5.63 ± 0.02 | 7.14 ± 0.02 | 0.35 ± 0.01 | 3.02 ± 0.01 | 0.82 ± 0.03 | 96 ± 1.00 | 4.33 ± 0.02 |

2.2. Biochar and Compost Characterization

While this study used pine residues exclusively, feedstock composition can strongly modulate the immobilization capacity of biochar. Lignocellulosic woods such as pine typically yield chars with low ash, moderate pH, and abundant oxygenated surface groups that favour complexation and electrostatic attraction of cationic metals; agricultural straws or manures, by contrast, produce biochars richer in mineral ash (Ca, Mg, P) that promote precipitation or co-precipitation mechanisms, often raising the pH beyond 9 [68]. We therefore selected pine to maximize functional-group-driven complexation and to avoid the very high electrical conductivity associated with manure biochars, which can impair seedling emergence in tailings. Future work will incorporate a side-by-side comparison of pine, crop-straw, and poultry-litter biochars produced at $500 \text{ }^\circ\text{C}$ to disentangle temperature and feedstock effects. The results of the characterization of biochar and compost are shown in Table 2.

Table 2. Physicochemical characterization of biochar and compost.

| Parameter | PB300 | PB500 | Compost |
|-----------------|-----------------|-----------------|--------------|
| C (%) | 72.27 ± 1.00 | 80.870 ± 1.589 | 20.92 ± 1.12 |
| H (%) | 4.22 ± 0.07 | 3.357 ± 0.124 | - |
| O (%) | 24.22 ± 1.00 | 17.887 ± 1.169 | - |
| N (%) | 0.460 ± 0.03 | 0.603 ± 0.025 | 1.79 ± 0.10 |
| S (%) | 0.017 ± 0.003 | 0.042 ± 0.006 | - |
| E.C. (uS/cm) | 169.433 ± 5.164 | 255.60 ± 10.923 | 11.29 ± 1.35 |
| TOM (%) | 54.597 ± 1.511 | 39.940 ± 2.359 | 35.02 ± 0.97 |
| pH | 7.133 ± 0.071 | 7.933 ± 0.012 | 8.53 ± 0.25 |
| CaO (%) | 0.147 ± 0.006 | 0.132 ± 0.007 | 3.60 ± 0.49 |
| MgO (%) | 0.052 ± 0.011 | 0.136 ± 0.038 | 0.64 ± 0.06 |
| H/C | 0.058 | 0.041 | - |
| O/C | 0.33 | 0.22 | - |
| NO ₃ | - | - | 13.55 ± 1.18 |
| NH ₄ | - | - | 1.35 ± 0.07 |

For pine biochar, as the temperature increased, the concentrations of carbon (C%), nitrogen (N%), and sulphur (S%) increased, while hydrogen (H%) and oxygen (O%) decreased. The physicochemical parameters are strongly influenced by the composition of the raw material, yet the variation in specific parameters generally follows a predictable trend with temperature. For example, as the pyrolysis temperature increases, the pH and surface area (m²/g) tend to rise, while the yield (%), hydrogen-to-carbon (H/C) ratio, and oxygen-to-carbon (O/C) ratio decrease [69]. Several pine-based studies indicate that the BET surface area rises from 300 °C to 500 °C ($\approx 2.9\text{--}175.4\text{ m}^2\text{ g}^{-1}$) but levels off—or even declines above 600 °C—due to sintering and higher ash content, while the functional groups that complex metals are progressively lost [70]. We therefore selected 500 °C in this study as the optimum compromise between specific surface area and chemical functionality.

The decrease in cation exchange capacity (CEC) observed in PB500 is attributed to the reduction in total organic matter (TOM) (39.940), as higher temperatures promote greater decomposition of organic material in the biomass. The lower CEC observed after pyrolysis at higher temperatures is also associated with a lower O/C ratio [71]. This is because higher temperatures lead to a decline in the abundance of functional groups, particularly oxygenated functional groups on the biochar surface [72]. The temperature-induced decrease in oxygen-containing surface functional groups may explain these findings [69]. Regarding pH, several studies have reported that increasing pyrolysis temperature leads to a rise in pH [72], which was also observed in this study, where the biochar exhibited a basic pH, like the findings of Cooper [73]. For electrical conductivity (EC), its value depends on the biomass type, but it generally increases with higher temperatures [74]. In this study, EC was 169.43 for PB300 and 255.60 for PB500. This increase may be attributed to higher ion mobility, reduced internal resistances, and increased thermal energy at elevated temperatures. The findings above illustrate the physicochemical properties of the compost, which exhibited a moderately alkaline pH (pH = 8.53) due to its composition. The low EC values in the following table are likely due to the minimal presence of soluble salts, which facilitates the composting process. The TOM content in the compost was lower compared to PBC300 and PBC500. Regarding the carbon-to-nitrogen (C/N) ratio, its value was lower (11.68:1), whereas it is considered optimal within the range of 25:1 to 30:1 [75]. A high C/N ratio leads to a decrease in biological activity, whereas a low C/N ratio results in nitrogen loss in the form of ammonia [76].

In Table 3, the heavy metal content in PBC300, PBC500, and compost was compared against various international regulations, including IBI [77], EBC [78], Germany (G), and Austria (AU) [79] for biochar, as well as standards from Korea, the EU, and the USA [80] for compost. Among these regulatory frameworks, the EBC and G standards appeared to be the most restrictive for heavy metal limits, particularly for cadmium (Cd) and lead (Pb), with

allowable concentrations set at ≤ 1.5 mg/kg and ≤ 150 mg/kg, respectively. Comparatively, AU and IBI standards were slightly more lenient, allowing higher concentrations for some metals. For PBC300 and PBC500, heavy metal levels were generally below the strictest thresholds, with cadmium and chromium being nearly undetectable, though arsenic (As) levels were relatively high, especially in PBC500 (24.453 mg/kg). The compost, derived from municipal waste in this research, exhibited higher concentrations of heavy metals such as Cu (54.94 mg/kg) and Zn (173.63 mg/kg), although within acceptable limits under USA and EU regulations. These findings suggest that while biochar from pine biomass adheres to most international biochar standards, compost quality may require stricter monitoring to comply with the most restrictive guidelines.

Table 3. Heavy metal characterization of biochar and compost with different international regulations.

| Heavy Metal | Biochar | | | | | Compost | | | | |
|-------------|-------------|---------|------------|------------|---------------------|---------------------|-------|----------|------|--------------------|
| | IBI | EBC | G | AU | PBC300 | PBC500 | Korea | EU | USA | Compost |
| As (mg/kg) | ≤ 100 | < 13 | ≤ 40 | ≤ 40 | 13.46 ± 0.772 | 24.453 ± 0.086 | 45 | 25 | 41 | 14.34 ± 0.48 |
| Cd (mg/kg) | ≤ 39 | < 1.5 | ≤ 1.5 | ≤ 3 | $< 0.0001 \pm 0.00$ | $< 0.0001 \pm 0.00$ | 5 | 0.7–10 | 39 | 2.23 ± 0.26 |
| Cr (mg/kg) | ≤ 1200 | < 90 | / | / | $< 0.0003 \pm 0.00$ | $< 0.0003 \pm 0.00$ | 200 | 70–200 | 1200 | 0.00021 ± 0.00 |
| Cu (mg/kg) | ≤ 6000 | < 100 | / | / | 0.0002 ± 0.00 | 0.8733 ± 0.086 | 360 | 70–600 | 1500 | 54.94 ± 2.32 |
| Pb (mg/kg) | 300 | < 150 | ≤ 150 | ≤ 100 | 0.0020 ± 0.001 | 0.0020 ± 0.000 | 130 | 70–1000 | 300 | 28.44 ± 2.31 |
| Ni (mg/kg) | ≤ 420 | < 50 | ≤ 80 | ≤ 100 | $< 0.0003 \pm 0.00$ | $< 0.0003 \pm 0.00$ | 45 | 20–200 | 420 | 0.00026 ± 0.00 |
| Zn (mg/kg) | ≤ 7400 | < 400 | / | / | 0.0001 ± 0.00 | 23.30 ± 3.176 | 900 | 210–4000 | 2800 | 173.63 ± 3.46 |

Figure S2 now not only identifies the principal FTIR bands but links them explicitly to the chemisorption and precipitation routes that account for the metal stabilization observed in Table S1 (Supplementary Materials). Broad bands at $3500\text{--}3250$ cm^{-1} (labelled O–H/N–H) originate from hydroxyl and amine groups whose lone-pair electrons donate empty d-orbitals of soft metals such as Cd^{2+} and Pb^{2+} , forming inner-sphere surface complexes [81]. The shoulder at $2500\text{--}2000$ cm^{-1} ($\text{C}\equiv\text{C}/\text{C}\equiv\text{O}$) reflects π -bond-rich alkynes and residual carbonyls that supply delocalized electrons for cation– π interactions, reinforcing Pb^{2+} sorption at circum-neutral pH [82]. The distinct peak near 1750 cm^{-1} ($\text{C}=\text{O}$) corresponds to carboxyl/ester carbonyls; deprotonation of $-\text{COOH}$ groups above pH 5 generates negatively charged sites that electrostatically attract Zn^{2+} and Ni^{2+} or chelate them as bidentate complexes [83]. The envelope at $1605\text{--}1660$ cm^{-1} ($\text{C}=\text{C}/-\text{CO}-\text{NH}-$) represents conjugated aromatics and amide linkages; the aromatic π -system provides additional cation– π adsorption, while amide carbonyls can coordinate Cu^{2+} via oxygen and nitrogen donors [84]. The smaller band at ≈ 1500 cm^{-1} ($\text{C}=\text{N}$) signals pyrrolic/hetero-aromatic N, whose basic lone pairs form strong coordination bonds with borderline metals (Cr^{3+} , Cu^{2+}) and contribute to Lewis-base sites on the char surface [85].

Comparison of spectra shows that PBC500 retains fewer O–H/N–H and more condensed $\text{C}=\text{C}/\text{C}=\text{N}$ structures than PBC300, indicating a shift from ligand-rich acidic sites toward π -electron-rich aromatic domains as pyrolysis rises from 300 °C to 500 °C; this transition favours inner-sphere complexation and cation– π interactions over simple ion exchange, explaining the superior immobilization of Pb, As, and Cd recorded for the 500 °C biochar treatments. Compost augments this effect by supplying additional $-\text{COOH}/\text{phenolic-OH}$ groups and raising soil pH, thereby promoting precipitation of metals as carbonates or phosphates and further reducing their bioavailability.

2.3. BCF and TF Results

The metal concentration results in the soil treatments (Table S1) show that arsenic levels ($204\text{--}412$ mg/kg) and lead levels ($1030\text{--}1811$ mg/kg) far exceed the limits set by all reviewed international standards, including Peru (50 mg/kg As and $70\text{--}140$ mg/kg Pb) [86], Canada (12 mg/kg As and $70\text{--}140$ mg/kg Pb) [87], the UE (300 mg/kg Pb) [88], and the Netherlands (intervention values: 55 mg/kg As and 530 mg/kg Pb), indicating severe contamination

that precludes any agricultural, residential, or even industrial use without prior remediation. Cadmium (9–16 mg/kg) exceeds agricultural thresholds (1.4–3 mg/kg) and, in some cases, residential limits (10 mg/kg), being acceptable only under industrial use (limit up to 22 mg/kg). Copper concentrations (86–136 mg/kg) exceed the values for agricultural and residential use (63–100 mg/kg) but remain below the Dutch intervention threshold (190 mg/kg). In contrast, chromium (4.6–4.8 mg/kg) and nickel (4.2–5.1 mg/kg) are well below international standards, complying with all regulations for any type of land use.

Across all treatments in Table 4, soils retained the highest metal concentrations, roots accumulated more than shoots, and TF values remained <0.40, confirming a phytostabilization rather than phytoextraction pattern. The root-to-soil BCFs we obtained are generally lower than those reported for maize grown with single amendments: for Pb, our maximum BCF (0.055, PBC500CP60) is below the 0.16 recorded for a rice husk biochar + poultry manure blend [51] and well under the 0.04–0.30 range observed for maize without compost [89]; TF-Pb values (<0.07) likewise undercut the 0.26 reported for biochar + poultry manure alone [90], indicating superior immobilization by the biochar–compost combination. For Cd, the highest BCF (0.084, run 12) is comparable to the 0.10–0.12 band cited for chars rich in oxygenated groups [50] but TF-Cd peaks (0.36, run 8) sit below the 0.50 threshold often associated with effective phytoextraction, mirroring the reduction in Cd mobility noted when biochar contains abundant surface O-functionalities [91]. Our As BCFs (≤ 0.059) resemble those achieved with biochar alone [92], yet TF-As remained ≤ 0.028 , reinforcing reports that the 500 °C char—through higher aromaticity and concomitantly greater microbial activity—favours As retention in roots while surface O-groups are diminished [93]. The porous biochar matrix and the labile-C supply from compost together create a buffered micro-habitat that enriches sulphate-reducing, phosphate-solubilizing, and exopolysaccharide-producing bacteria [94]; these consortia immobilize metals by precipitating Pb and As as sulphides [95] or metal-phosphate minerals and by entrapping Cd and Zn in biofilms, further lowering their mobility [96]. The quinone-rich surfaces of the char act as electron shuttles, accelerating microbial redox conversions such as As (V) \rightarrow As (III) and Cr (VI) \rightarrow Cr (III), which yield less-soluble species that are readily sorbed on the char–compost complex [97]. In contrast, Zn, Cu, and Cr displayed moderate BCFs (Zn ≤ 0.066 , Cu ≤ 0.141 , Cr ≤ 0.135) far below those reported for maize with high-dose single amendments (BCF_Zn 0.82; BCF_Cu 1.08; BCF_Cr 0.21) [49]; their TF maxima (Zn 0.39, Cu 0.39, Cr 0.49) occurred at the lowest tailings dose and 300 °C, underscoring that milder pyrolysis preserves oxygenated functional groups together with microbially exuded organic ligands that facilitate upward metal transport. These comparisons show that combining compost with pine-derived biochar shifts the system toward metal immobilization, particularly at 500 °C and 60% tailings, whereas milder chars (300 °C) paired with lower tailings promote limited translocation trends consistent with the literature but delivering overall safer shoot concentrations.

Table 4. Experimental results of BFC and TF for As, Cd, Pb, Cr, Ni, and Cu in corn (*Zea mays* L.), under different tailings doses and pyrolysis temperatures.

| Run | B: Pyrolysis Temperature °C | A: Doses Mining Tailing % (w/w) | FBC-As | FT-As | FBC-Cd | FT-Cd | FBC-Pb | FT-Pb | FBC-Cr | FT-Cr | FBC-Ni | FT-Ni | FBC-Cu | FT-Cu |
|-----|-----------------------------|---------------------------------|--------|-------|--------|-------|--------|-------|--------|-------|--------|-------|--------|-------|
| 1 | 500 | 30 | 0.012 | 0.023 | 0.018 | 0.182 | 0.015 | 0.011 | 0.101 | 0.208 | 0.043 | 0.217 | 0.035 | 0.111 |
| 2 | 500 | 60 | 0.059 | 0.004 | 0.068 | 0.043 | 0.037 | 0.006 | 0.100 | 0.222 | 0.070 | 0.147 | 0.122 | 0.018 |
| 3 | 300 | 60 | 0.015 | 0.011 | 0.019 | 0.229 | 0.022 | 0.011 | 0.109 | 0.260 | 0.074 | 0.171 | 0.066 | 0.079 |
| 4 | 300 | 30 | 0.039 | 0.022 | 0.013 | 0.308 | 0.005 | 0.040 | 0.066 | 0.313 | 0.047 | 0.250 | 0.014 | 0.290 |
| 5 | 300 | 60 | 0.015 | 0.010 | 0.024 | 0.154 | 0.029 | 0.010 | 0.090 | 0.239 | 0.072 | 0.167 | 0.066 | 0.067 |
| 6 | 500 | 30 | 0.008 | 0.037 | 0.018 | 0.316 | 0.011 | 0.029 | 0.087 | 0.225 | 0.048 | 0.316 | 0.053 | 0.067 |
| 7 | 500 | 30 | 0.010 | 0.028 | 0.030 | 0.190 | 0.012 | 0.017 | 0.077 | 0.314 | 0.048 | 0.300 | 0.055 | 0.198 |
| 8 | 300 | 30 | 0.023 | 0.017 | 0.015 | 0.364 | 0.004 | 0.039 | 0.113 | 0.240 | 0.071 | 0.267 | 0.019 | 0.224 |
| 9 | 300 | 60 | 0.018 | 0.012 | 0.024 | 0.212 | 0.020 | 0.013 | 0.058 | 0.385 | 0.038 | 0.294 | 0.053 | 0.125 |
| 10 | 300 | 30 | 0.023 | 0.015 | 0.013 | 0.308 | 0.004 | 0.034 | 0.097 | 0.488 | 0.071 | 0.400 | 0.019 | 0.394 |
| 11 | 500 | 60 | 0.045 | 0.004 | 0.077 | 0.030 | 0.064 | 0.006 | 0.135 | 0.318 | 0.112 | 0.164 | 0.124 | 0.017 |
| 12 | 500 | 60 | 0.049 | 0.004 | 0.084 | 0.035 | 0.064 | 0.003 | 0.119 | 0.400 | 0.099 | 0.200 | 0.141 | 0.024 |

2.4. Effect of Study Parameters

Root-level patterns (Supplementary Material Figure S3–S6): For every metal except Ni, the Root BCF rises sharply when tailings are doubled from 30% to 60%, and values are always higher with 500 °C biochar than with 300 °C; the greatest jumps occur for Cu and Cd, confirming that high-temperature biochar markedly enhances below-ground retention. Shoot-level patterns: TF generally falls as tailings increase, indicating restricted movement to aerial parts at higher contamination; 300 °C biochar maintains higher TF for Cd, Pb, Ni, and Cu, whereas 500 °C favours As (only at 30%) and Cr (at 60%), showing that the temperature effect is metal-specific. The three-dimensional plots corroborate the 2D trends of BCF maxima for the As, Cd, Ni, and Cu cluster at the extreme combination of 500 °C + 60% tailings, while Pb and Cr respond more moderately, suggesting distinct sorption/complexation behaviour. Translocation surfaces: TFs for As, Cd, Ni, and Cu decline steadily with both factors, Pb shows only a slight drop, and Cr remains low overall; collectively, these surfaces confirm that elevated pyrolysis temperature combined with higher tailings load consistently shifts metal distribution toward the root compartment.

2.5. Factor Model Analysis

According to the ANOVA results presented in Table 5, the BCF model for As is highly significant ($F = 27.74$, $p < 0.0001$). Both the tailings dose ($p = 0.0003$) and the pyrolysis temperature ($p = 0.046$), as well as their interaction ($p = 0.0002$), significantly affect arsenic accumulation in maize roots. Similarly, Cd shows an even stronger response ($F = 82.12$, $p < 0.0001$), where all factors—tailings dose, pyrolysis temperature, and the interaction—are highly significant (all $p < 0.0001$), underscoring Cd's heightened sensitivity to changes in both pyrolysis conditions and contamination levels. For Pb, the overall model is also significant ($F = 21.93$, $p = 0.0003$). Tailings dose ($p = 0.0002$), pyrolysis temperature ($p = 0.0029$), and their interaction ($p = 0.0387$) all contribute notably, although the effect magnitudes are somewhat lower than for Cd. In contrast, Cr does not exhibit any statistically significant effect ($F = 1.56$, $p = 0.2741$), indicating that within the tested ranges, neither the proportion of tailings nor the pyrolysis temperature (nor their synergy) appreciably alters Cr accumulation in roots. Ni's model is significant ($F = 4.41$, $p = 0.0415$). Here, tailings dose ($p = 0.0422$) and the interaction term ($p = 0.0323$) emerge as key drivers of Ni accumulation, while pyrolysis temperature alone is not significant ($p = 0.2684$). These findings show that As, Cd, Pb, and Ni accumulation in maize roots is each influenced to varying degrees by the tailings dose and pyrolysis temperature, whereas Cr appears largely unaffected under the conditions evaluated.

Table 6 clarifies which factor effects are statistically meaningful ($\alpha = 0.05$). For As, the overall TF model is highly significant ($F = 22.36$, $p = 0.0003$); both tailings dose ($p = 0.0003$) and its interaction with pyrolysis temperature ($p = 0.0037$) contribute, whereas temperature alone is non-significant ($p = 0.377$). Cd likewise shows a significant model ($F = 21.18$, $p = 0.0004$), with independent main-factor effects from dose ($p = 0.0003$) and temperature ($p = 0.001$), but a non-significant interaction ($p = 0.249$), indicating additive rather than synergistic control. Pb follows a similar pattern: significant model ($F = 24.35$, $p = 0.0002$), significant main factors (dose $p = 0.0001$; temperature $p = 0.002$), and an interaction that trends toward but does not reach significance ($p = 0.063$). By contrast, Cr shows no significant model or factor effects ($F = 0.60$, $p = 0.654$), and Ni is marginal overall ($F = 2.95$, $p = 0.098$) with only a weak dose effect ($p = 0.037$). Cu exhibits a clearly significant model ($F = 13.72$, $p = 0.0016$); both dose ($p = 0.0004$) and temperature ($p = 0.0052$) act independently, while their interaction remains non-significant ($p = 0.141$). These statistics confirm that metal translocation is chiefly governed by tailings dose across most elements, augmented by pyrolysis temperature for Cd, Pb, and Cu, with synergistic dose-temperature effects evident only for As.

Table 5. ANOVA for BCF of As, Cd, Pb, Cr, Ni, and Cu in *Zea mays* L. under different mining tailings doses and pyrolysis temperatures.

| Source | Sum of Squares | df | Mean Square | F-Value | p-Value |
|--|----------------|----|-------------|---------|---------|
| BFC-As = $0.026 + 0.007 \times A + 0.004 \times B + 0.014 \times AB$ | | | | | |
| Model | 0.003 | 3 | 0.001 | 27.74 | 0.0001 |
| A-Mine Tailings Dosage | 0.0006 | 1 | 0.0006 | 16.83 | 0.0034 |
| B-Pyrolysis Temperature | 0.0002 | 1 | 0.0002 | 5.57 | 0.046 |
| AB | 0.0022 | 1 | 0.0022 | 60.8 | <0.0001 |
| Pure Error | 0.0003 | 8 | 0 | | |
| Cor Total | 0.0033 | 11 | | | |
| BFC-Cd = $0.034 + 0.0159 \times A + 0.0157 \times B + 0.012 \times AB$ | | | | | |
| Model | 0.0075 | 3 | 0.0025 | 82.12 | <0.0001 |
| A-Mine Tailings Dosage | 0.003 | 1 | 0.003 | 98.59 | <0.0001 |
| B-Pyrolysis Temperature | 0.003 | 1 | 0.003 | 96.69 | <0.0001 |
| AB | 0.0016 | 1 | 0.0016 | 51.09 | <0.0001 |
| Pure Error | 0.0002 | 8 | 0 | | |
| Cor Total | 0.0078 | 11 | | | |
| BFC-Pb = $0.024 + 0.015 \times A + 0.009 \times B + 0.006 \times AB$ | | | | | |
| Model | 0.0044 | 3 | 0.0015 | 21.99 | 0.0003 |
| A-Mine Tailings Dosage | 0.0028 | 1 | 0.0028 | 41.94 | 0.0002 |
| B-Pyrolysis Temperature | 0.0012 | 1 | 0.0012 | 17.94 | 0.0029 |
| AB | 0.0004 | 1 | 0.0004 | 6.1 | 0.0387 |
| Pure Error | 0.0005 | 8 | 0.0001 | | |
| Cor Total | 0.0049 | 11 | | | |
| BFC-Cr = $0.096 + 0.006 \times A + 0.008 \times B + 0.009 \times AB$ | | | | | |
| Model | 0.002 | 3 | 0.0007 | 1.56 | 0.2741 |
| A-Mine Tailings Dosage | 0.0004 | 1 | 0.0004 | 0.9484 | 0.3586 |
| B-Pyrolysis Temperature | 0.0006 | 1 | 0.0006 | 1.44 | 0.2647 |
| AB | 0.001 | 1 | 0.001 | 2.28 | 0.1695 |
| Pure Error | 0.0034 | 8 | 0.0004 | | |
| Cor Total | 0.0054 | 11 | | | |
| BFC-Ni = $0.066 + 0.0116 \times A + 0.004 \times B + 0.012 \times AB$ | | | | | |
| Model | 0.0036 | 3 | 0.0012 | 4.41 | 0.0415 |
| A-Mine Tailings Dosage | 0.0016 | 1 | 0.0016 | 5.83 | 0.0422 |
| B-Pyrolysis Temperature | 0.0002 | 1 | 0.0002 | 0.7126 | 0.4231 |
| AB | 0.0018 | 1 | 0.0018 | 6.68 | 0.0323 |
| Pure Error | 0.0022 | 8 | 0.0003 | | |
| Cor Total | 0.0057 | 11 | | | |
| BFC-Cu = $0.064 + 0.031 \times A + 0.024 \times B + 0.009 \times AB$ | | | | | |
| Model | 0.0201 | 3 | 0.0067 | 91.1 | <0.0001 |
| A-Mine Tailings Dosage | 0.0119 | 1 | 0.0119 | 161.47 | <0.0001 |
| B-Pyrolysis Temperature | 0.0072 | 1 | 0.0072 | 97.52 | <0.0001 |
| AB | 0.0011 | 1 | 0.0011 | 14.32 | 0.0054 |
| Pure Error | 0.0006 | 8 | 0.0001 | | |
| Cor Total | 0.0207 | 11 | | | |

Table 6. ANOVA for TF of As, Cd, Pb, Cr, Ni, and Cu in *Zea mays* L. under different tailings doses and biochar pyrolysis temperatures.

| Source | Sum of Squares | df | Mean Square | F-Value | p-Value |
|--|----------------|----|-------------|---------|---------|
| TF-As = $0.015 + -0.008 \times A + 0.001 \times B + -0.005 \times AB$ | | | | | |
| Model | 0.0011 | 3 | 0.0004 | 22.36 | 0.0003 |
| A-Mine Tailings Dosage | 0.0008 | 1 | 0.0008 | 49.75 | 0.0001 |
| B-Pyrolysis Temperature | 0 | 1 | 0 | 0.8755 | 0.3768 |
| AB | 0.0003 | 1 | 0.0003 | 16.45 | 0.0037 |
| Pure Error | 0.0001 | 8 | 0 | | |
| Cor Total | 0.0012 | 11 | | | |
| TF-Cd = $0.197 + -0.080 \times A + -0.06 \times B + -0.016 \times AB$ | | | | | |
| Model | 0.131 | 3 | 0.0437 | 21.18 | 0.0004 |
| A-Mine Tailings Dosage | 0.0775 | 1 | 0.0775 | 37.58 | 0.0003 |
| B-Pyrolysis Temperature | 0.0503 | 1 | 0.0503 | 24.42 | 0.0011 |
| AB | 0.0032 | 1 | 0.0032 | 1.54 | 0.2493 |
| Pure Error | 0.0165 | 8 | 0.0021 | | |
| Cor Total | 0.1475 | 11 | | | |
| TF-Pb = $0.018 + -0.010 \times A + -0.006 \times B + 0.0035 \times AB$ | | | | | |
| Model | 0.0018 | 3 | 0.0006 | 24.35 | 0.0002 |
| A-Mine Tailings Dosage | 0.0012 | 1 | 0.0012 | 49.53 | 0.0001 |
| B-Pyrolysis Temperature | 0.0005 | 1 | 0.0005 | 18.86 | 0.0025 |
| AB | 0.0001 | 1 | 0.0001 | 4.67 | 0.0627 |
| Pure Error | 0.0002 | 8 | 0 | | |
| Cor Total | 0.002 | 11 | | | |

Table 6. Cont.

| Source | Sum of Squares | df | Mean Square | F-Value | p-Value |
|---|----------------|----|-------------|---------|---------|
| TF-Cr = 0.300 + 0.003 × A + −0.019 × B + 0.029 × AB | | | | | |
| Model | 0.0151 | 3 | 0.005 | 0.5957 | 0.6353 |
| A-Mine Tailings Dosage | 0.0001 | 1 | 0.0001 | 0.0131 | 0.9116 |
| B-Pyrolysis Temperature | 0.0047 | 1 | 0.0047 | 0.5574 | 0.4767 |
| AB | 0.0102 | 1 | 0.0102 | 1.22 | 0.3021 |
| Pure Error | 0.0674 | 8 | 0.0084 | | |
| Cor Total | 0.0825 | 11 | | | |
| TF-Ni = 0.241 + −0.050 × A + −0.017 × B + −0.003 × AB | | | | | |
| Model | 0.0343 | 3 | 0.0114 | 2.95 | 0.0984 |
| A-Mine Tailings Dosage | 0.0307 | 1 | 0.0307 | 7.91 | 0.0227 |
| B-Pyrolysis Temperature | 0.0035 | 1 | 0.0035 | 0.901 | 0.3703 |
| AB | 0.0001 | 1 | 0.0001 | 0.0306 | 0.8655 |
| Pure Error | 0.031 | 8 | 0.0039 | | |
| Cor Total | 0.0653 | 11 | | | |
| TF-Cu = 0.135 + −0.079 × A + −0.062 × B + 0.027 × AB | | | | | |
| Model | 0.1306 | 3 | 0.0435 | 13.72 | 0.0016 |
| A-Mine Tailings Dosage | 0.076 | 1 | 0.076 | 23.94 | 0.0012 |
| B-Pyrolysis Temperature | 0.0461 | 1 | 0.0461 | 14.53 | 0.0052 |
| AB | 0.0085 | 1 | 0.0085 | 2.68 | 0.1405 |
| Pure Error | 0.0254 | 8 | 0.0032 | | |
| Cor Total | 0.156 | 11 | | | |

Based on the statistical indicators in Table 7, the Root Bioconcentration Factor (BCF) and Translocation Factor (TF) models for As, Cd, Pb, and Cu exhibit robust fits, as evidenced by high R^2 values (≥ 0.84), closely aligned adjusted and predicted R^2 values, and Adeq Precision well above 4, indicating strong explanatory and predictive capabilities. Arsenic (As) presents R^2 values of 0.91 (BCF) and 0.89 (TF), while Cd's BCF model stands out with an R^2 of 0.97 and a predicted R^2 of 0.93. Lead (Pb) shows values near 0.90 for both BCF and TF, though with slightly higher C.V. (above 27%), implying somewhat greater variability. Copper (Cu) also achieves excellent results ($R^2 = 0.97$ for BCF, $R^2 = 0.84$ for TF), confirming that the tested factors of biochar pyrolysis temperature and tailings dose effectively explain both root accumulation and shoot translocation for these metals. In contrast, chromium (Cr) and nickel (Ni) display weaker or even negative adjusted R^2 values, along with substantially lower predicted R^2 , suggesting that the chosen experimental ranges do not sufficiently capture the variables governing their uptake and translocation. Overall, these findings highlight the reliability of the factorial model for As, Cd, Pb, and Cu under the studied conditions, while indicating that additional parameters or an expanded experimental range may be required to better account for Cr and Ni behaviour.

Table 7. Statistical indicators (ANOVA) of the factorial models of the Root Bioconcentration Factor (BCF) and the Translocation Factor (TF) for As, Cd, Pb, Cr, Ni, and Cu.

| Model Indicators | BFC-As | TF-As | BFC-Cd | TF-Cd | BFC-Pb | TF-Pb | BFC-Cr | TF-Cr | BFC-Ni | TF-Ni | BFC-Cu | TF-Cu |
|------------------|--------|-------|--------|-------|--------|-------|--------|-------|--------|-------|--------|-------|
| R^2 | 0.91 | 0.89 | 0.97 | 0.89 | 0.89 | 0.90 | 0.37 | 0.18 | 0.62 | 0.53 | 0.97 | 0.84 |
| Adjusted R^2 | 0.88 | 0.85 | 0.96 | 0.85 | 0.85 | 0.86 | 0.13 | −0.12 | 0.48 | 0.35 | 0.96 | 0.78 |
| Predicted R^2 | 0.80 | 0.76 | 0.93 | 0.75 | 0.76 | 0.78 | −0.42 | −0.84 | 0.15 | −0.07 | 0.94 | 0.63 |
| Adeq Precision | 11.90 | 11.11 | 19.76 | 11.07 | 10.71 | 11.38 | 2.71 | 1.85 | 5.00 | 3.76 | 22.58 | 8.70 |
| Std. Dev. | 0.01 | 0.00 | 0.01 | 0.05 | 0.01 | 0.00 | 0.02 | 0.09 | 0.02 | 0.06 | 0.01 | 0.06 |
| Mean | 0.03 | 0.02 | 0.03 | 0.20 | 0.02 | 0.02 | 0.10 | 0.30 | 0.07 | 0.24 | 0.06 | 0.13 |
| C.V.% | 22.87 | 25.77 | 16.46 | 22.99 | 34.25 | 27.25 | 21.59 | 30.49 | 24.86 | 25.82 | 13.43 | 41.86 |

Because the aerial tissues accumulated up to 0.39 mg kg^{−1} Cd and 0.065 mg kg^{−1} Pb, direct use as fodder or food is not advisable. Two end-of-life routes are therefore recommended. (i) Thermochemical valorization: Controlled slow pyrolysis (≤ 550 °C) converts the biomass into a secondary biochar whose ash-enriched fraction retains >90% of the sequestered metals; the resulting char can be encapsulated in asphalt or concrete, a practice already permitted under Peruvian technical guidance. (ii) Bioenergy with ash capture: Gasification or pelletized combustion yields heat/steam while concentrating metals in

<5% of the original mass; the ash can be stabilized with ordinary Portland cement and disposed of in Class I landfills. Both pathways meet Basel Convention recommendations for contaminated phytomass and close the carbon loop by generating energy.

3. Materials and Methods

3.1. Mine Tailing Sampling and Physicochemical Characterization

The tailings were sampled in Quiulacocho, considering a representative sample from four points, as shown in Figure S7, and taking into consideration the procedure carried out by the Ministry of the Environment in Peru [98]. The analysis of heavy metals was conducted after drying the mining tailings at 60 °C for 24 h [99]. The total heavy metal analysis was carried out using the ICP Aqua Regia Digestion technique.

3.2. Biochar and Compost Production

For the production of biochar, pine forest residues from the Cutervo district at the province of Cajamarca in Peru were obtained (6°22'31.19" S, 78°48'6.90" WO), as shown in Figure S1. Forest residues of pine were cut and then dried in an oven at 105 °C for 24 h [100]. The pine biochar was produced at two temperatures (300 °C and 500 °C) for 1.5 h. The biochar was named PBC300 and PBC500, and they were produced in a stainless-steel pyrolytic oven at 15 °C/min, as shown in Figure S8. The oven had a capacity of 5 L, and it had two appropriate circle endings (b) with the aim to dissipate heat. This oven also had a manometer that could register pressure from 0 to 7 bar (0–100 psi) (c), and it had a thermometer that could register an adequate temperature. Furthermore, there was a valve to regulate the gas outlet (e). Biochar yield was determined by Equation (1). The compost was produced in composting piles for three months, and the biomass to produce compost was from organic waste, such as fruits and pruning wastes from parks. It was made at the Municipality of Pueblo Libre in the district of Pueblo Libre (12°04'36.83" S, 77°03'24.61" W), in the province of Lima, Peru.

$$Yield (\%) = \frac{W_{Final}}{W_{initial}} \times 100 \quad (1)$$

where W_{final} = biomass (kg) of the pine biochar after the pyrolysis; $W_{initial}$ = biomass (kg) of pine before the pyrolysis. Biochar and compost were granulated through mechanical sieving using a U.S.A. Standard Testing Sieve (ASTM No. 20, 850 µm) to achieve a uniform particle size distribution suitable for subsequent application (Figure S9).

3.3. Biochar and Compost Physicochemical Characterization

For PBC300, PBC500, and compost, pH and electrical conductivity (E.C.) (dS/m) were assessed with the methodology of Rajkovich [101] using a multiparameter (Multiparameter HANNA HI2020-02). To determine MgO and CaO, an atomic absorption spectrophotometer was used (BIOBASE-BK-AA320N) [102].

To evaluate heavy metals, such as As, Cd, Cr, Cu, Pb, Hg, Ni, and Zn (mg/kg), we used an ICP—mass spectrometry (THERMO SCIENTIFIC XSERIES 2 ICPMS), and the results were compared with international regulations. With respect to total organic matter (TOM), samples were dried at 105 °C for 10 h in desiccator, then burned at 550 °C for 6 h in muffle, and the total organic matter content was gained by the weight difference with the content of ash [103].

The elemental composition of PBC300 and PB500 (C (%), H (%), O (%), N (%), S (%)) followed the reference method of ASTM D5373 [104], using a carbon analyzer (CHN628). FTIR infrared spectroscopy analysis was performed to determine the impact of pyrolytic temperature on the conversion of functional groups on the surface of PBC300 and PBC500, for

which an infrared spectrophotometer was used (Perkin Elmer Spectrum 10, wavenumber range 380 cm^{-1} to 4000 cm^{-1}) [105].

In addition, in compost, total carbon (TC) was determined using the ASTM D5373 reference method [104]. Total nitrogen (TN) content was determined as follows: 1 g samples were dissolved in a certain amount of distilled water in addition to 1.2 g, 0.4 mL (1 M), and 5 mL 98%, and the total nitrogen content was measured using the Kjeldahl method [106]. Calcium and magnesium were analyzed by shaking 1 g of compost sample with sodium acetate solution for 1 h prior to atomic absorption spectroscopy detection (Varian Spectra AA 220FS, USA). The $\text{N} - \text{NH}_4^+$ and $\text{N} - \text{NO}_3^-$ amounts were extracted with 2 M of KCl [107] and determined by the AA3 Continuous Flow Analytical System. All analyses were performed in triplicate ($n = 3$), and the standard error (SE) was calculated.

3.4. Operation of the Phytoremediation System

For the ex situ phytoremediation design, four treatments were evaluated, as shown in Table 8. Each pot contained a total of 3 kg of substrate, with 3% *w/w* of biochar and 1.8% *w/w* of compost added to all treatments. This mixture was prepared uniformly for all four treatments with a tailings dose of 30% *w/w* and 60% *w/w* [108], while the remaining portion consisted of uncontaminated soil. Each treatment was coded as shown in Table 8. Direct seeding was performed with three seeds of *Zea mays* L. per experimental unit. Soil moisture conditions were maintained, as the plant requires appropriate water levels. Therefore, distilled water was used, and irrigation was applied continuously and consistently every two days [109] with an equal volume for all treatments until sample collection for laboratory analysis. Irrigation in each experimental unit was always carried out at field capacity, preventing the generation of leachates.

Table 8. Factorial design.

| Biochar | Compost | Mining Tailing (% <i>w/w</i>) | Component | Codification |
|---------|---------|--------------------------------|---------------------------|--------------|
| PBC300 | YES | 30% | Soil + <i>Zea mays</i> L. | PBC300CP30 |
| PBC300 | YES | 60% | Soil + <i>Zea mays</i> L. | PBC300CP60 |
| PBC500 | YES | 30% | Soil + <i>Zea mays</i> L. | PBC500CP30 |
| PBC500 | YES | 60% | Soil + <i>Zea mays</i> L. | PBC500CP60 |

3.5. Experimental Design

A 2×2 factorial design was used (Table 8), in which two main factors were combined: the mining tailings dose (30% *w/w* and 60% *w/w*) and the pyrolysis temperature of pine biochar (300 °C and 500 °C). Each combination of these two factors was replicated three times, resulting in a total of twelve experimental runs, conducted in a randomized order. For each treatment, compost was incorporated, and maize (*Zea mays* L.) was cultivated. The response variables measured were the BCF and the TF for different metals.

3.6. Bioconcentration and Translocation Factors

The calculation of the Bioconcentration Factor (BCF) was used to assess the phys-
tabilization of *Zea mays* L. The equation used for BCF calculation has been previously documented [110], and it is as follows:

$$\text{BCF} = \frac{\text{Concentration of metal in plant root}}{\text{Concentration of metal in soil}} \quad (2)$$

The assessment of the Translocation Factor (TF) plays a crucial role in assessing the metabolic functions and well-being of individuals plants that thrive in polluted environments [111]. TF was determined by the ratio of metal concentration in plant aerial parts (shoot) and metal concentration in plant roots [112], and the equation was the following:

$$TF = \frac{\text{Metal concentration in plant shoot}}{\text{Metal concentration in plant root}} \quad (3)$$

3.7. Statistical Analysis

For this research, a factorial design was developed as a statistical regression tool. This method allows for a mathematical relationship between the response variable (Y) and the independent variables (X_1 , X_2 , X_3), as shown in the following equation:

$$Y = \beta_0 + \beta_1 X_1 + \beta_2 X_2 + \beta_3 X_3 + \beta_{12} X_1 X_2 + \beta_{13} X_1 X_3 + \beta_{23} X_2 X_3 + \beta_{123} X_1 X_2 X_3 \quad (4)$$

where Y is the predicted response used as the dependent variable; X_i ($i = 1, 2$, and 3) represents the parameters; β_0 can be calculated by dividing the system responses (Y) by the total number of observations, including those conducted at the central point; and β_i ($i = 1, 2$, and 3) and β_{ij} ($i = 1, 2$, and 3 ; $j = 1, 2$, and 3) represent the effect coefficients [1].

Subsequently, an analysis of variance (ANOVA) was conducted to evaluate the quality and robustness of the fitted models for each response variable. The R^2 (coefficient of determination) represents the proportion of variation explained by the model, while the adjusted R^2 corrects for the number of model terms to prevent overestimation. The predicted R^2 assesses the model's generalization ability by indicating how much variability is explained when applied to new data. Adeq Precision (Adequate Precision) measures the signal-to-noise ratio, with values above 4 considered sufficient for distinguishing real effects from experimental noise. The standard deviation (Std. Dev.) quantifies residual dispersion (differences between observed and predicted values), while the mean helps interpret this dispersion relative to the average value. Lastly, the coefficient of variation (C.V.%) relates the standard deviation to the mean, serving as an indicator of whether residual variability is high or low in relative terms.

4. Conclusions

The results of this study demonstrate that the combined application of biochar and compost significantly enhances the remediation of mine tailing-contaminated soils. This factorial study demonstrates that co-amending mine tailing-contaminated soil with 3% w/w pine-derived biochar and 1.8% w/w compost markedly improves substrate pH, cation exchange capacity, and nutrient retention while reducing the bioavailability and shoot translocation of priority metals (As, Cd, Pb, Cu, Cr, Ni). The combination of the higher tailings load (60%) with the hotter char (500 °C) achieved the greatest immobilization, keeping Translocation Factors below 0.07 for Pb and <0.03 for As. Future work will (i) upscale the study to field conditions, first establishing maize and then an additional short-cycle food crop to quantify yields and whole-plant metal uptake under ambient climate and irrigation; (ii) incorporate BET surface area determinations and test chars produced at ≥ 600 °C to assess whether any extra porosity gained offsets the concurrent loss of surface functional groups; (iii) benchmark maize against regionally native hyper-accumulator species, alone and in mixed-cropping schemes, to identify synergistic combinations; (iv) track metal speciation, soil enzymatic activity, and rhizosphere microbiome composition across successive cropping cycles to verify the long-term chemical and biological stability of the remediation strategy; and (v) translate the findings into policy by providing baseline thresholds and amendment-rate guidelines that can inform national soil quality standards and regional land use regulations, thereby supporting evidence-based decisions for the safe rehabilitation and productive reuse of mine-affected soils.

Supplementary Materials: The following supporting information can be downloaded at: <https://www.mdpi.com/article/10.3390/plants14101448/s1>. Figure S1. Location of the pine harvesting site and municipal composting plant. Figure S2. FTIR analysis of biochar (PBC300 (a) and PBC500 (b)). Figure S3. Interaction of Mining Tailings Dose and Pine Biochar Pyrolysis Temperature on BCF for heavy metals. Figure S4. Interaction of Mining Tailings Dose and Pine Biochar Pyrolysis Temperature on TF for heavy metals. Figure S5. 3D Response Surfaces of BCF for As, Cd, Pb, Cr, Ni, and Cu as a Function of Biochar Pyrolysis Temperature and Mining Tailings Dose. Figure S6. 3D Response Surfaces of TF for As, Cd, Pb, Cr, Ni, and Cu as a Function of Biochar Pyrolysis Temperature and Mining Tailings Dose. Figure S7. Location of sampling points at the Quiulacochoa mining tailings in Pasco. Figure S8. Compost and biochar production. Figure S9. Granulation of biochar and compost using ASTM No. 20 sieve. Table S1. BCF and TF of the treatments.

Author Contributions: Conceptualization, P.V.-V. and J.S.-V.; methodology, T.C.Q.-O. and M.F.C.-C.; software, A.P.-N.; validation, A.A.-P., L.L.O.-G. and J.S.-V.; formal analysis, F.T.-C.; investigation, P.V.-V.; resources, P.V.-V.; data curation, E.N.-B.; writing—original draft preparation, P.V.-V.; writing—review and editing, R.A.-A.; visualization, Y.V.-Z.; supervision, C.T.M.-S. and P.V.-V.; project administration, J.S.-V.; funding acquisition, P.V.-V. All authors have read and agreed to the published version of the manuscript.

Funding: This research received no external funding.

Data Availability Statement: All the data are included in the manuscript.

Conflicts of Interest: The authors have no competing interests to declare.

References

- Shi, Y.; Zang, Y.; Yang, H.; Zhang, X.; Shi, J.; Zhang, J.; Liu, B. Biochar enhanced phytostabilization of heavy metal contaminated mine tailings: A review. *Front. Environ. Sci.* **2022**, *10*, 1044921. [[CrossRef](#)]
- Ai, Y.; Wang, Y.; Song, L.; Hong, W.; Zhang, Z.; Li, X.; Zhou, S.; Zhou, J. Effects of biochar on the physiology and heavy metal enrichment of *Vetiveria zizanioides* in contaminated soil in mining areas. *J. Hazard. Mater.* **2023**, *448*, 130965. [[CrossRef](#)] [[PubMed](#)]
- Vasuki, Y.; Yu, L.; Holden, E.J.; Kovesi, P.; Wedge, D.; Grigg, A.H. The spatial-temporal patterns of land cover changes due to mining activities in the Darling Range, Western Australia: A Visual Analytics Approach. *Ore. Geol. Rev.* **2019**, *108*, 23–32. [[CrossRef](#)]
- Gasco, G.; Alvarez, M.L.; Paz-Ferreiro, J.; Mendez, A. Combining phytoextraction by *Brassica napus* and biochar amendment for the remediation of a mining soil in Riotinto (Spain). *Chemosphere* **2019**, *231*, 562–570. [[CrossRef](#)]
- Ngole-Jeme, V.M.; Fantke, P. Ecological and human health risks associated with abandoned gold mine tailings contaminated soil. *PloS ONE* **2017**, *12*, e0172517. [[CrossRef](#)]
- Fernández-Macías, J.C.; González-Mille, D.J.; García-Arreola, M.E.; Cruz-Santiago, O.; Rivero-Pérez, N.E.; Pérez-Vázquez, F.; Ilizaliturri-Hernández, C.A. Integrated probabilistic risk assessment in sites contaminated with arsenic and lead by long-term mining liabilities in San Luis Potosi, Mexico. *Ecotoxicol. Environ. Saf.* **2020**, *197*, 110568. [[CrossRef](#)]
- Ramírez, M.G.V.; Barrantes, J.A.G.; Thomas, E.; Miranda, L.A.G.; Pillaca, M.; Peramas, L.D.T.; Tapia, L.R.B. Heavy metals in alluvial gold mine spoils in the peruvian amazon. *Catena* **2020**, *189*, 104454. [[CrossRef](#)]
- Ramírez, M.G.V.; Ruiz, C.M.V.; Gomringer, R.C.; Pillaca, M.; Thomas, E.; Stewart, P.M.; Miranda, L.A.G.; Dañobeytia, F.R.; Barrantes, J.A.G.; Gushiken, M.C. Mercury in soils impacted by alluvial gold mining in the Peruvian Amazon. *J. Environ. Manag.* **2021**, *288*, 112364. [[CrossRef](#)]
- Salgado-Almeida, B.; Falquez-Torres, D.A.; Romero-Crespo, P.L.; Valverde-Armas, P.E.; Guzmán-Martínez, F.; Jiménez-Oyola, S. Risk assessment of mining environmental liabilities for their categorization and prioritization in gold-mining areas of Ecuador. *Sustainability* **2022**, *14*, 6089. [[CrossRef](#)]
- Cruzado-Tafur, E.; Torró, L.; Bierla, K.; Szpunar, J.; Tauler, E. Heavy metal contents in soils and native flora inventory at mining environmental liabilities in the Peruvian Andes. *J. South Am. Earth Sci.* **2021**, *106*, 103107. [[CrossRef](#)]
- Rodríguez-Zapata, M.A.; Ruiz-Agudelo, C.A. Environmental liabilities in Colombia: A critical review of current status and challenges for a megadiverse country. *Environ. Chall.* **2021**, *5*, 100377. [[CrossRef](#)]
- Lam, E.J.; Cánovas, M.; Gálvez, M.E.; Montofré, Í.L.; Keith, B.F.; Faz, Á. Evaluation of the phytoremediation potential of native plants growing on a copper mine tailing in northern Chile. *J. Geochem. Explor.* **2017**, *182*, 210–217. [[CrossRef](#)]
- Maboeta, M.S.; Oladipo, O.G.; Botha, S.M. Ecotoxicity of mine tailings: Unrehabilitated versus rehabilitated. *Bull Environ. Contam. Toxicol.* **2018**, *100*, 702–707. [[CrossRef](#)]

14. Rosas-Ramírez, M.; Tovar-Sánchez, E.; Rodríguez-Solís, A.; Flores-Trujillo, K.; Castrejón-Godínez, M.L.; Mussali-Galante, P. Assisted phytoremediation between biochar and *Crotalaria pumila* to phytostabilize heavy metals in mine tailings. *Plants* **2024**, *13*, 2516. [CrossRef]
15. Chen, H.; Tang, L.; Wang, Z.; Su, M.; Tian, D.; Zhang, L.; Li, Z. Evaluating the protection of bacteria from extreme Cd (II) stress by P-enriched biochar. *Environ. Pollut.* **2020**, *263*, 114483. [CrossRef]
16. Ali, H.; Khan, E. Trophic transfer, bioaccumulation, and biomagnification of non-essential hazardous heavy metals and metalloids in food chains/webs—Concepts and implications for wildlife and human health. *Hum. Ecol. Risk Assess. Int. J.* **2019**, *25*, 1353–1376. [CrossRef]
17. Sheoran, V.; Sheoran, A.S.; Poonia, P. Soil reclamation of abandoned mine land by revegetation: A review. *Int. J. Soil Sediment Water* **2010**, *3*, 13.
18. Clemente, R.; Walker, D.J.; Pardo, T.; Martínez-Fernández, D.; Bernal, M.P. The use of a halophytic plant species and organic amendments for the remediation of a trace elements-contaminated soil under semi-arid conditions. *J. Hazard. Mater.* **2012**, *223*, 63–71. [CrossRef]
19. Guo, L.; Liu, J.; Chen, Y.; Zhang, X. Remediation of high concentration chromium contaminated soil by Enhanced Electrodynamics Method. *Earth Sci. Res. J.* **2021**, *25*, 247–253. [CrossRef]
20. Huang, M.; Zhu, Y.; Li, Z.; Huang, B.; Luo, N.; Liu, C.; Zeng, G. Compost as a soil amendment to remediate heavy metal-contaminated agricultural soil: Mechanisms, efficacy, problems, and strategies. *Water Air Soil Pollut.* **2016**, *227*, 359. [CrossRef]
21. Medyńska-Juraszek, A.; Ćwieląg-Piasecka, I. Effect of biochar application on heavy metal mobility in soils impacted by copper smelting processes. *Pol. J. Environ. Stud.* **2020**, *29*, 1749–1757. [CrossRef] [PubMed]
22. Xiang, L.; Sheng, H.; Gu, C.; Marc, R.G.; Wang, Y.; Bian, Y.; Jiang, X.; Wang, F. Biochar combined with compost to reduce the mobility, bioavailability and plant uptake of 2, 2', 4, 4'-tetrabrominated diphenyl ether in soil. *J. Hazard. Mater.* **2019**, *374*, 341–348. [CrossRef] [PubMed]
23. Nie, X.; Huang, X.; Li, M.; Lu, Z.; Ling, X. Advances in Soil Amendments for Remediation of Heavy Metal-Contaminated Soils: Mechanisms, Impact, and Future Prospects. *Toxics* **2024**, *12*, 872. [CrossRef] [PubMed]
24. Oldfield, T.L.; Sikirica, N.; Mondini, C.; López, G.; Kuikman, P.J.; Holden, N.M. Biochar, compost and biochar-compost blend as options to recover nutrients and sequester carbon. *J. Environ. Manag.* **2018**, *218*, 465–476. [CrossRef]
25. Jindo, K.; Suto, K.; Matsumoto, K.; García, C.; Sonoki, T.; Sanchez-Monedero, M.A. Chemical and biochemical characterisation of biochar-blended composts prepared from poultry manure. *Bioresour. Technol.* **2012**, *110*, 396–404. [CrossRef]
26. Agegnehu, G.; Bass, A.M.; Nelson, P.N.; Bird, M.I. Benefits of biochar, compost and biochar-compost for soil quality, maize yield and greenhouse gas emissions in a tropical agricultural soil. *Sci. Total Environ.* **2016**, *543*, 295–306. [CrossRef]
27. Agegnehu, G.; Srivastava, A.K.; Bird, M.I. The role of biochar and biochar-compost in improving soil quality and crop performance: A review. *Appl. Soil Ecol.* **2017**, *119*, 156–170. [CrossRef]
28. Fan, X.; Wei, Y.; Song, D.; Zhou, T.; Li, R.; Su, X.; Zhang, T.; Cheng, S.; Xiao, R. Biochar enhanced co-composting for peat-free seedling substrate: A win-win solution for sustainable development of modern vegetable industry. *Process Saf. Environ. Prot.* **2025**, *194*, 1504–1514. [CrossRef]
29. Shi, G.; Li, H.; Fu, Q.; Li, T.; Hou, R.; Chen, Q.; Xue, P. Effects of biochar and compost on the abundant and rare microbial communities assembly and multifunctionality in pesticide-contaminated soil under freeze-thaw cycles. *Environ. Pollut.* **2024**, *362*, 125003. [CrossRef]
30. Yu, Z.; Zhou, M.; Zhang, H.; Yuan, L.; Lv, P.; Wang, L.; Zhang, J. Changes in Cd forms and Cd resistance genes in municipal sludge during coupled earthworm and biochar composting. *Ecotoxicol. Environ. Saf.* **2024**, *286*, 117179. [CrossRef]
31. Etim, E.E. Phytoremediation and its mechanisms: A review. *Int. J. Env. Bioenergy* **2012**, *2*, 120–136.
32. Robinson, B.H.; Anderson, C.W.N.; Dickinson, N.M. Phytoextraction: Where's the action? *J. Geochem. Explor.* **2015**, *151*, 34–40. [CrossRef]
33. Alkorta, I.; Becerril, J.M.; Garbisu, C. Phytostabilization of metal contaminated soils. *Rev. Environ. Health* **2010**, *25*, 135–146. [CrossRef] [PubMed]
34. Alsafran, M.; Saleem, M.H.; Rizwan, M.; Al Jabri, H.; Usman, K.; Fahad, S. An overview of heavy metals toxicity in plants, tolerance mechanism, and alleviation through lysine-chelation with micro-nutrients—A novel approach. *Plant Growth Regul.* **2023**, *100*, 337–354. [CrossRef]
35. Falcon Estrella, J.V. Fitoextracción De Metales Pesados En Suelo Contaminado Con *Zea mays* L. En La Estación Experimental El Mantaro-Junín En El Año 2016. 2017. Available online: <https://repositorio.uncp.edu.pe/handle/20.500.12894/4611> (accessed on 10 February 2025).
36. Adejumo, A.L.; Azeez, L.; Kolawole, T.O.; Aremu, H.K.; Adedotun, I.S.; Oladeji, R.D.; Adeleke, A.E.; Abdullah, M. Silver nanoparticles strengthen *Zea mays* against toxic metal-related phytotoxicity via enhanced metal phytostabilization and improved antioxidant responses. *Int. J. Phytoremediation* **2023**, *25*, 1676–1686. [CrossRef]

37. Atta, M.I.; Zehra, S.S.; Ali, H.; Ali, B.; Abbas, S.N.; Aimen, S.; Sarwar, S.; Ahmad, I.; Hussain, M.; Al-Ashkar, I. Assessing the effect of heavy metals on maize (*Zea mays* L.) growth and soil characteristics: Plants-implications for phytoremediation. *PeerJ* **2023**, *11*, e16067. [CrossRef]
38. Ahmad, M.; Usman, A.R.A.; Al-Faraj, A.S.; Ahmad, M.; Sallam, A.; Al-Wabel, M.I. Phosphorus-loaded biochar changes soil heavy metals availability and uptake potential of maize (*Zea mays* L.) plants. *Chemosphere* **2018**, *194*, 327–339. [CrossRef]
39. Rosas-Castor, J.M.; Guzmán-Mar, J.L.; Hernández-Ramírez, A.; Garza-González, M.T.; Hinojosa-Reyes, L.J.S. Arsenic accumulation in maize crop (*Zea mays*): A review. *Sci. Total Environ.* **2014**, *488*, 176–187. [CrossRef]
40. Campos, H.; Caligari, P.D.S. *Genetic Improvement of Tropical Crops*; Springer: Berlin/Heidelberg, Germany, 2017; Volume 661.
41. Aladesanmi, O.T.; Oroboade, J.G.; Osisioogu, C.P.; Osewole, A.O. Bioaccumulation factor of selected heavy metals in *Zea mays*. *J. Heal Pollut.* **2019**, *9*, 191207. [CrossRef]
42. Pandey, J.; Sarkar, S.; Pandey, V.C. Compost-assisted phytoremediation. In *Assisted Phytoremediation*; Elsevier: Amsterdam, The Netherlands, 2022; pp. 243–264.
43. Virú-Vásquez, P.; Pardavé, R.H.; Coral, M.F.C.; Bravo-Toledo, L.; Curaqueo, G. Biochar and Compost in the Soil: A Bibliometric Analysis of Scientific Research. *Environ. Res. Eng. Manag.* **2022**, *78*, 73–95. [CrossRef]
44. Novak, J.M.; Ippolito, J.A.; Watts, D.W.; Sigua, G.C.; Ducey, T.F.; Johnson, M.G. Biochar compost blends facilitate switchgrass growth in mine soils by reducing Cd and Zn bioavailability. *Biochar* **2019**, *1*, 97–114. [CrossRef] [PubMed]
45. Sigua, G.C.; Novak, J.M.; Watts, D.W.; Ippolito, J.A.; Ducey, T.F.; Johnson, M.G.; Spokas, K.A. Phytostabilization of Zn and Cd in mine soil using corn in combination with biochars and manure-based compost. *Environments* **2019**, *6*, 69. [CrossRef]
46. Alidou-Arzika, I.; Lebrun, M.; Miard, F.; Nandillon, R.; Bayçu, G.; Bourgerie, S.; Morabito, D. Assessment of compost and three biochars associated with *Ailanthus altissima* (Miller) Swingle for lead and arsenic stabilization in a post-mining Technosol. *Pedosphere* **2021**, *31*, 944–953. [CrossRef]
47. Máthé-Gáspár, G.; Anton, A. Phytoremediation study: Factors influencing heavy metal uptake of plants. *Acta Biol. Szeged.* **2005**, *49*, 69–70.
48. Korentajer, L. A Review of the Agricultural Use of Sewage Sludge: Benefits and Potential Hazards. 1991. Available online: <https://www.cabidigitallibrary.org/doi/full/10.5555/19911961563> (accessed on 23 April 2025).
49. Alaboudi, K.A.; Ahmed, B.; Brodie, G. Effect of biochar on Pb, Cd and Cr availability and maize growth in artificial contaminated soil. *Ann. Agric. Sci.* **2019**, *64*, 95–102. [CrossRef]
50. Irfan, M.; Mudassir, M.; Khan, M.J.; Dawar, K.M.; Muhammad, D.; Mian, I.A.; Ali, W.; Fahad, S.; Saud, S.; Hayat, Z. Heavy metals immobilization and improvement in maize (*Zea mays* L.) growth amended with biochar and compost. *Sci. Rep.* **2021**, *11*, 18416. [CrossRef]
51. Rashid, M.S.; Liu, G.; Yousaf, B.; Song, Y.; Ahmed, R.; Rehman, A.; Arif, M.; Irshad, S.; Cheema, A.I. Efficacy of rice husk biochar and compost amendments on the translocation, bioavailability, and heavy metals speciation in contaminated soil: Role of free radical production in maize (*Zea mays* L.). *J. Clean Prod.* **2022**, *330*, 129805. [CrossRef]
52. Kaur, H.; Katal, P.; Chandel, S.; Singh, D.; Kumar, P.; Choudhary, M. Microbes mediated alleviation of chromium (Cr VI) stress for improved phytoextraction in fodder maize (*Zea mays* L.) cultivar. *Heliyon* **2024**, *10*, e40361. [CrossRef]
53. Bashir, M.A.; Naveed, M.; Ashraf, S.; Mustafa, A.; Ali, Q.; Rafique, M.; Alamri, S.; Siddiqui, M.H. Performance of *Zea mays* L. cultivars in tannery polluted soils: Management of chromium phytotoxicity through the application of biochar and compost. *Physiol. Plant* **2021**, *173*, 129–147. [CrossRef]
54. Sun, C.; Wang, D.; Shen, X.; Li, C.; Liu, J.; Lan, T.; Wang, W.; Xie, H.; Zhang, Y. Effects of biochar, compost and straw input on root exudation of maize (*Zea mays* L.): From function to morphology. *Agric. Ecosyst. Environ.* **2020**, *297*, 106952. [CrossRef]
55. Ch'ng, H.Y.; Ahmed, O.H.; Majid, N.M.A. Biochar and compost influence the phosphorus availability, nutrients uptake, and growth of maize (*Zea mays* L.) in tropical acid soil. *Pak. J. Agric. Sci.* **2014**, *51*, 797–806.
56. Rehman, M.Z.; Rizwan, M.; Ali, S.; Fatima, N.; Yousaf, B.; Naeem, A.; Sabir, M.; Ahmad, H.R.; Ok, Y.S. Contrasting effects of biochar, compost and farm manure on alleviation of nickel toxicity in maize (*Zea mays* L.) in relation to plant growth, photosynthesis and metal uptake. *Ecotoxicol. Environ. Saf.* **2016**, *133*, 218–225. [CrossRef] [PubMed]
57. Glick, B.R.; Glick, B.R. Phytoremediation. In *Beneficial Plant-Bacterial Interactions*; Springer: Berlin/Heidelberg, Germany, 2020; pp. 319–359.
58. Astete, J.; Cáceres, W.; Gastañaga Mdel, C.; Lucero, M.; Sabastizagal, I.; Oblitas, T.; Pari, J.; Rodríguez, F. Intoxicación por plomo y otros problemas de salud en niños de poblaciones aledañas a relaves mineros. *Rev. Peru. Med. Exp. Salud. Pública* **2009**, *26*, 15–19.
59. Barreto-Pio, C.; Bravo-Toledo, L.; Virú-Vásquez, P.; Borda-Contreras, A.; Zarate-Sarapura, E.; Pilco, A. Optimization Applying Response Surface Methodology in the Co-treatment of Urban and Acid Wastewater from the Quiulacocha Lagoon, Pasco (Peru). *Environ. Res. Eng. Manag.* **2023**, *79*, 90–109. [CrossRef]
60. Baylón Coritoma, M.; Roa Castro, K.; Libio Sánchez, T.; Tapia Ugaz, L.; Jara Pena, E.; Macedo Prada, D.; Salvatierra Sevillano, A.; Dextre Rubina, A. Evaluación de la diversidad de algas fitoplanctónicas como indicadores de la calidad del agua en lagunas altoandinas del departamento de Pasco (Perú). *Ecol. Apl.* **2018**, *17*, 119–132. [CrossRef]

61. INDECI. Reporte De Peligro Inminente N° 115–14/5/2021/COEN–INDECI/23:00 Horas (Reporte N° 5) Por Desembalse De La Relavera Quiulacocho En El Distrito De Simón Bolívar-Pasco-Indeci Tarea De Todos 2021. 2023. Available online: <https://portal.indeci.gob.pe/emergencias/reporte-de-peligro-inminente-n-055-25-2-2021-coen-indeci-1450-horas-reporte-n-1-por-desembalse-de-la-relavera-quiulacocho-en-el-distrito-de-simon-bolivar-pasco/> (accessed on 10 February 2025).
62. INDECI Reporte Complementario No 2130–28/2/2023/COEN–INDECI/16:30 Horas (Reporte N° 2) Lluvias Intensas En El Distrito De Paucartambo-Pasco-INDECI Tarea De Todos 2023. 2023. Available online: <https://www.desdeadentro.pe/2022/03/lluvias-y-granizadas-extreman-ponen-en-riesgo-de-colapso-a-relavera-quiulacocho-en-pasco/> (accessed on 10 February 2025).
63. Dold, B.; Wade, C.; Fontboté, L. Water management for acid mine drainage control at the polymetallic Zn-Pb-(Ag-Bi-Cu) deposit Cerro de Pasco, Peru. *J. Geochem. Explor.* **2009**, *100*, 133–141. [[CrossRef](#)]
64. Urbano Paccho, G.G. Remoción De Manganeso Por Procesos De Ozonización En Drenajes Ácidos De Mina De La Relavera Quiulacocho, Cerro de Pasco, 2022. 2023. Available online: <https://hdl.handle.net/20.500.13084/8394> (accessed on 10 February 2025).
65. Sarathchandra, S.S.; Rengel, Z.; Solaiman, Z.M. A review on remediation of Iron ore mine tailings via organic amendments coupled with phytoremediation. *Plants* **2023**, *12*, 1871. [[CrossRef](#)]
66. Romero, F.M.; Armienta, M.A.; Gutiérrez, M.E.; Villasenor, G. Geological and climatic factors determining hazard and environmental impact of mine tailings. *Rev. Int. Contam. Ambient.* **2008**, *24*, 43–54.
67. Fashola, M.O.; Ngole-Jeme, V.M.; Babalola, O.O. Physicochemical properties, heavy metals, and metal-tolerant bacteria profiles of abandoned gold mine tailings in Krugersdorp, South Africa. *Can. J. Soil Sci.* **2020**, *100*, 217–233. [[CrossRef](#)]
68. Palacios-Hugo, R.; Calle-Maravi, J.; Césare-Coral, M.F.; Iparraguirre, J.; Virú-Vásquez, P. Physicochemical Characterization and Stability of Biochar Obtained from 5 Species of Forest Biomass in Peru. *Environ. Res. Eng. Manag.* **2023**, *79*, 33–51. [[CrossRef](#)]
69. Nkoh, J.N.; Ajibade, F.O.; Atakpa, E.O.; Abdulaha-Al Baquy, M.; Mía, S.; Odii, E.C.; Xu, R. Reduction of heavy metal uptake from polluted soils and associated health risks through biochar amendment: A critical synthesis. *J. Hazard. Mater. Adv.* **2022**, *6*, 100086. [[CrossRef](#)]
70. Kim, K.H.; Kim, J.Y.; Cho, T.S.; Choi, J.W. Influence of pyrolysis temperature on physicochemical properties of biochar obtained from the fast pyrolysis of pitch pine (*Pinus rigida*). *Bioresour. Technol.* **2012**, *118*, 158–162. [[CrossRef](#)] [[PubMed](#)]
71. Mukherjee, A.; Zimmerman, A.R.; Harris, W. Surface chemistry variations among a series of laboratory-produced biochars. *Geoderma* **2011**, *163*, 247–255. [[CrossRef](#)]
72. Roshan, A.; Ghosh, D.; Maiti, S.K. How temperature affects biochar properties for application in coal mine spoils? A meta-analysis. *Carbon Res.* **2023**, *2*, 3. [[CrossRef](#)]
73. Cooper, J.; Greenberg, I.; Ludwig, B.; Hippich, L.; Fischer, D.; Glaser, B.; Kaiser, M. Effect of biochar and compost on soil properties and organic matter in aggregate size fractions under field conditions. *Agric. Ecosyst. Environ.* **2020**, *295*, 106882. [[CrossRef](#)]
74. Rehrach, D.; Reddy, M.R.; Novak, J.M.; Bansode, R.R.; Schimmel, K.A.; Yu, J.; Watts, D.W.; Ahmedna, M. Production and characterization of biochars from agricultural by-products for use in soil quality enhancement. *J. Anal. Appl. Pyrolysis.* **2014**, *108*, 301–309. [[CrossRef](#)]
75. Jia, H.; Chu, D.; You, X.; Li, Y.; Huang, C.; Zhang, J.; Zeng, X.; Yao, H.; Zhou, Z. Biochar improved the composting quality of seaweeds and cow manure mixture and altered the microbial community. *Front. Microbiol.* **2022**, *13*, 1064252. [[CrossRef](#)]
76. Becker, S.J.; Ebrahimzadeh, A.; Plaza Herrada, B.M.; Lao, M.T. Characterization of compost based on crop residues: Changes in some chemical and physical properties of the soil after applying the compost as organic amendment. *Commun. Soil Sci. Plant Anal.* **2010**, *41*, 696–708. [[CrossRef](#)]
77. IBI. Standardized product definition and product testing guidelines for biochar that is used in soil. *Int. Biochar. Initiat.* **2015**, *23*. Available online: https://biochar-international.org/wp-content/uploads/2020/06/IBI_Biochar_Standards_V2.1_Final2.pdf (accessed on 23 April 2025).
78. EBC. European Biochar Certificate (EBC)—Guidelines Version 6.1. 2015 [Cited 15 March 2022]. Available online: https://www.researchgate.net/publication/278727508_European_Biochar_Certificate_EBC_-_guidelines_version_61?channel=doi&linkId=5584728c08ae71f6ba8c4cdf&showFulltext=true (accessed on 10 February 2025).
79. Meyer, S.; Genesisio, L.; Vogel, I.; Schmidt, H.P.; Soja, G.; Someus, E.; Shackley, S.; Verheijen, F.; Glaser, B. Biochar Standardization and Legislation Harmonization. *J. Environ. Eng. Landsc. Manag.* **2015**, *25*, 175–191. [[CrossRef](#)]
80. Cho, W.M.; Ravindran, B.; Kim, J.K.; Jeong, K.H.; Lee, D.J.; Choi, D.Y. Nutrient status and phytotoxicity analysis of goat manure discharged from farms in South Korea. *Environ. Technol.* **2017**, *38*, 1191–1199. [[CrossRef](#)] [[PubMed](#)]
81. Younis, U.; Rahi, A.A.; Danish, S.; Ali, M.A.; Ahmed, N.; Datta, R.; Fahad, S.; Holatko, J.; Hammerschmidt, T.; Brtnicky, M.; et al. Fourier Transform Infrared Spectroscopy vibrational bands study of *Spinacia oleracea* and *Trigonella corniculata* under biochar amendment in naturally contaminated soil. *PLoS ONE* **2021**, *16*, e0253390. [[CrossRef](#)] [[PubMed](#)]
82. Selvarajoo, A.; Wong, Y.L.; Khoo, K.S.; Chen, W.H.; Show, P.L. Biochar production via pyrolysis of citrus peel fruit waste as a potential usage as solid biofuel. *Chemosphere* **2022**, *294*, 133671. [[CrossRef](#)] [[PubMed](#)]
83. Lam, S.S.; Liew, R.K.; Lim, X.Y.; Ani, F.N.; Jusoh, A. Fruit waste as feedstock for recovery by pyrolysis technique. *Int. Biodeterior. Biodegrad.* **2016**, *113*, 325–333. [[CrossRef](#)]

84. Zhang, X.; Zhao, B.; Liu, H.; Zhao, Y.; Li, L. Effects of pyrolysis temperature on biochar's characteristics and speciation and environmental risks of heavy metals in sewage sludge biochars. *Environ. Technol. Innov.* **2022**, *26*, 102288. [CrossRef]
85. Cuixia, Y.; Yingming, X.; Lin, W.; Xuefeng, L.; Yuebing, S.; Hongtao, J. Effect of different pyrolysis temperatures on physico-chemical characteristics and lead (ii) removal of biochar derived from chicken manure. *RSC Adv.* **2020**, *10*, 3667–3674. [CrossRef]
86. MINAN. Glosario De Términos Sitios Contaminados. Minist del Ambient. 2016; 17. Available online: <https://www.gob.pe/institucion/minam/informes-publicaciones/2650-glosario-de-terminos-sitios-contaminados> (accessed on 23 April 2025).
87. CEPA. *Canadian Soil Quality Guidelines for the Protection of Environmental and Human Health*; Canadian Council of Ministers of the Environment: Winnipeg, MB, Canada, 2007.
88. Directive, C. 86/609/EEC of 24 November 1986 on the approximation of laws, regulations and administrative provisions of the Member States regarding the protection of animals used for experimental and other scientific purposes. *Off J. Eur. Commun.* **1986**, *29*, L358.
89. Munive, R.; Loli, O.; Azabache, A.; Gamarra, G. Phytoremediation with corn (*Zea mays* L.) and Stevia compost on soils degraded by contamination with heavy metals. *Sci. Agropecu.* **2018**, *9*, 551–560. [CrossRef]
90. Liu, L.; Li, J.; Wu, G.; Shen, H.; Fu, G.; Wang, Y. Combined effects of biochar and chicken manure on maize (*Zea mays* L.) growth, lead uptake and soil enzyme activities under lead stress. *PeerJ* **2021**, *9*, e11754. [CrossRef]
91. Navas-Cárdenas, C.; Caetano, M.; Endara, D.; Jiménez, R.; Lozada, A.B.; Manangón, L.E.; Navarrete, A.; Reinoso, C.; Sommer-Márquez, A.E.; Villasana, Y. The Role of Oxygenated Functional Groups on Cadmium Removal using Pyrochar and Hydrochar Derived from *Guadua angustifolia* Residues. *Water* **2023**, *15*, 525. [CrossRef]
92. Alam, M.Z.; Hoque, M.A.; Ahammed, G.J.; Carpenter-Boggs, L. Effects of arbuscular mycorrhizal fungi, biochar, selenium, silica gel, and sulfur on arsenic uptake and biomass growth in *Pisum sativum* L. *Emerg. Contam.* **2020**, *6*, 312–322. [CrossRef]
93. Liao, W.; Zhang, X.; Ke, S.; Shao, J.; Yang, H.; Zhang, S.; Chen, H. Effect of different biomass species and pyrolysis temperatures on heavy metal adsorption, stability and economy of biochar. *Ind. Crops Prod.* **2022**, *186*, 115238. [CrossRef]
94. Dissanayaka Mudiyanse, T. Effects of Biochar on Heavy Metal Bioavailability and Microbial Properties in Contaminated Soils. Ph.D. Thesis, La Trobe University, Sydney, Australia, 2021.
95. Wu, Z.; Firmin, K.A.; Cheng, M.; Wu, H.; Si, Y. Biochar enhanced Cd and Pb immobilization by sulfate-reducing bacterium isolated from acid mine drainage environment. *J. Clean Prod.* **2022**, *366*, 132823. Available online: <https://www.sciencedirect.com/science/article/pii/S0959652622024180> (accessed on 10 February 2025). [CrossRef]
96. Zhao, Z.; Jiang, G.; Mao, R. Effects of particle sizes of rock phosphate on immobilizing heavy metals in lead zinc mine soils. *J. Soil Sci. Plant Nutr.* **2014**, *14*, 258–266. [CrossRef]
97. Ren, J.; Huang, H.; Zhang, Z.; Xu, X.; Zhao, L.; Qiu, H.; Cao, X. Enhanced microbial reduction of Cr (VI) in soil with biochar acting as an electron shuttle: Crucial role of redox-active moieties. *Chemosphere* **2023**, *328*, 138601. [CrossRef]
98. MINAM. Guia para el Muestreo de Suelos. 2014. Available online: <https://www.gob.pe/institucion/minam/informes-publicaciones/2702-guia-para-muestreo-de-suelos> (accessed on 23 April 2025).
99. Sarker, S.K.; Bruckard, W.; Haque, N.; Roychand, R.; Bhuiyan, M.; Pramanik, B.K. Characterization of a carbonatite-derived mining tailing for the assessment of rare earth potential. *Process Saf. Environ. Prot.* **2023**, *173*, 154–162. [CrossRef]
100. Chen, X.; Zhang, R.; Zhao, B.; Fan, G.; Li, H.; Xu, X.; Zhang, M. Preparation of porous biochars by the co-pyrolysis of municipal sewage sludge and hazelnut shells and the mechanism of the nano-zinc oxide composite and Cu (II) adsorption kinetics. *Sustainability* **2020**, *12*, 8668. [CrossRef]
101. Rajkovich, S.; Enders, A.; Hanley, K.; Hyland, C.; Zimmerman, A.R.; Lehmann, J. Corn growth and nitrogen nutrition after additions of biochars with varying properties to a temperate soil. *Biol. Fertil. Soils* **2012**, *48*, 271–284. [CrossRef]
102. Hofmeister, A.M.; Keppel, E.; Speck, A.K. Absorption and reflection infrared spectra of MgO and other diatomic compounds. *Mon. Not. R Astron. Soc.* **2003**, *345*, 16–38. [CrossRef]
103. Jiménez, E.I.; García, V.P. Relationships between organic carbon and total organic matter in municipal solid wastes and city refuse composts. *Bioresour. Technol.* **1992**, *41*, 265–272. [CrossRef]
104. LECO Corporation. Carbon, Hydrogen, and Nitrogen in Coal 2013. 2013 [Cited 8 November 2022]. Available online: <https://knowledge.leco.com/results/application-note-carbon-hydrogen-nitrogen-in-coke-using-chn828-629/viewdocument/1910> (accessed on 10 February 2025).
105. Santos, R.V.; Mendes, M.A.A.; Alexandre, C.; Carrott, M.R.; Rodrigues, A.; Ferreira, A.F. Assessment of biomass and biochar of maritime pine as a porous medium for water retention in soils. *Energies* **2022**, *15*, 5882. [CrossRef]
106. Hamoda, M.F.; Qdais, H.A.A.; Newham, J. Evaluation of municipal solid waste composting kinetics. *Resour. Conserv. Recycl.* **1998**, *23*, 209–223. [CrossRef]
107. Cao, T.; Meng, J.; Liang, H.; Yang, X.; Chen, W. Can biochar provide ammonium and nitrate to poor soils?: Soil column incubation. *J. Soil Sci. Plant Nutr.* **2017**, *17*, 253–265. [CrossRef]
108. Jara-Peña, E.; Gómez, J.; Montoya, H.; Chanco, M.; Mariano, M.; Cano, N. Capacidad fitoremediadora de cinco especies altoandinas de suelos contaminados con metales pesados. *Rev. Peru. Biol.* **2014**, *21*, 145–154. [CrossRef]

109. Barandiarán Gamarra, M.Á. Manual Técnico Del Cultivo De Maíz Amarillo Duro. 2020. Available online: <https://repositorio.inia.gob.pe/items/dae3e96f-ae5e-4857-868e-00fb6b308684> (accessed on 10 February 2025).
110. Yoon, J.; Cao, X.; Zhou, Q.; Ma, L.Q. Accumulation of Pb, Cu, and Zn in native plants growing on a contaminated Florida site. *Sci. Total Environ.* **2006**, *368*, 456–464. [[CrossRef](#)]
111. Chandra, R.; Yadav, S.; Yadav, S. Phytoextraction potential of heavy metals by native wetland plants growing on chlorolignin containing sludge of pulp and paper industry. *Ecol. Eng.* **2017**, *98*, 134–145. [[CrossRef](#)]
112. Gupta, A.K.; Sinha, S. Decontamination and/or revegetation of fly ash dykes through naturally growing plants. *J. Hazard. Mater.* **2008**, *153*, 1078–1087. [[CrossRef](#)]

Disclaimer/Publisher’s Note: The statements, opinions and data contained in all publications are solely those of the individual author(s) and contributor(s) and not of MDPI and/or the editor(s). MDPI and/or the editor(s) disclaim responsibility for any injury to people or property resulting from any ideas, methods, instructions or products referred to in the content.